Electrophoretic Deposition of Al/CuO Energetic Materials and Their Heat Release Performance

Miao He [1], Yuting Xie[1], Jie Ni[1], Yan Jian[1], Shaoyi Song[1], Hebin Bao[2], Xuzhong Zeng[1],
Xueming Li[1,], Qihui Wang[1,3,*]*

[1] School of Chemistry and Chemical Engineering, Chongqing University, Chongqing 400044, China
[2] Army logistical University of PLA, Chongqing 401311, China
[3] Institute for Health and Environment, Chongqing University of Science and Technology, Chongqing
401331, China
*E-mail: lxm301@cqu.edu.cn (Xueming Li), qihuiwang@cqu.edu.cn (Qihui Wang)

In this study, Al/CuO energetic materials with high exothermic properties were prepared by electrophoretic deposition of nano-Al and CuO microboxes on Ti sheets. The microstructure and phase composition of Al/CuO energetic materials were characterized by scanning electron microscopy (SEM) and X-ray diffraction (XRD). The electrophoretic deposition behavior of nano-Al and CuO microboxes were systematically investigated, and the electrophoretic deposition process was controlled by diffusion. The differential scanning calorimetry results showed that the maximum heat released by Al/CuO energetic material is 3049 J/g at an equivalent ratio of 3.0. The combustion properties of Al/CuO energetic materials were tested by optical fiber spectra. When the equivalence ratio was 2.25, the intensity of the spectra of Al/CuO energetic materials were the strongest and the lowest color temperature was 2916 K. This work provides a reference for the preparation of highly exothermic Al/CuO energetic materials by electrophoretic deposition.

1. INTRODUCTION

In the past few years, energetic materials, composed of fuel (Al or Mg) and oxidizer (CuO, Fe_2O_3, MnO_2, MoO_3, NiO, etc.), have attracted great attention due to their outstanding heat release and rapid combustion rate [1-9]. Energetic materials have great potential applications in the fields of propellants, explosives, gas generators, welding and ignition materials [10-20]. It is of great practical value to integrate energetic materials into energetic semiconductor bridges (SCB) by micro-electro-mechanical system (MEMS) technology [21].

Electrophoretic deposition (EPD) can make stable suspended particles migrate in the electric field and deposite dense films on the electrodes. EPD has been widely used in the fields of coating and catalytic materials [22-24]. Specifically, the EPD method can prepare an energetic film on the surface of various conductive materials such as Cu, Ni, Ti and stainless steel. A great deal of efforts have been devoted to fabricating different types of energetic materials including Al/Fe_2O_3, Al/MoO_3, Al/CuO and exploring their exothermic properties [21, 25-28]. However, the investigation of the EPD mechanism of energetic materials is still not clear.

This work demonstrates the preparation of high-exothermic Al/CuO energetic materials on Ti electrodes by EPD method and the EPD kinetics of Al/CuO energetic materials. The exothermic behavior and optical fiber spectrum of the sample were systematically studied by differential scanning calorimetry (DSC) and spectrometer. These Al/CuO energetic materials exhibit excellent exothermic properties. This work provides valuable guidance for preparation of highly exothermic Al/CuO energetic materials.

2. EXPERIMENTAL SECTION

2.1 Materials and sample preparation

The nano–Al (100 nm) and polyethyleneimine (PEI, Mw=10,000) were purchased from Aladdin Reagent Co., Ltd. (Shanghai, China). $Cu(CH_3COO)_2 \cdot H_2O$, NaOH, glucose, citric acid (CA), sodium dodecyl sulfonate (SDS), sodium dodecylbenzene sulfonate (SDBS) and isopropanol were purchased from Kelong Industrial Inc., China. Sodium lauryl sulfate (SLS) was acquired from Sinopharm Chemical Reagent Co., Ltd. All chemicals were of analytical grade and used directly without further purification.

The CuO microboxes were fabricated according to the previous report [29]. In a typical synthesis, 1.25 g of $Cu(CH_3COO)_2 \cdot H_2O$ was dissolved in 100 mL of deionized water under vigorous magnetic stirring for 15 min at 65 °C. Then, 1.63 g NaOH and 1.50 g glucose were added to the above solution quickly. After stirring for 30 min, the red Cu_2O was filtered and washed several times with distilled water and absolute ethanol, respectively. Finally, the CuO was obtained by calcining the Cu_2O at 600 °C for 12 h.

2.2 Electrophoretic deposition kinetics

In a typical electrophoresis, solid particles (Al, CuO) with a total mass concentration of 0.1 g/L were added to isopropanol, then the additive was added. The solution was mixed by ultrasonic dispersion for 0.5 h to form a stable suspension. In all the electrophoresis process, the titanium sheets were used as both anode and cathode, set parallel to each other with a distance of 1 cm and immersed into the suspension. Subsequently, the solid particles were deposited at a certain filed strength and deposition time. Finally, the deposition amount was measured by weighing the Ti electrodes before and after EPD by a precision balance.

The charge on the surface of nanoparticles has an important influence on the electrophoretic deposition behavior. The additive can be selectively adsorbed to the surface of the nanoparticles by

electrostatic action, changing the surface charge of the nanoparticles. As the nano-Al particles can be easily deposited on the Ti sheet even without any additive, only the effects of surfactants on the electrophoretic deposition behavior of CuO cubes were investigated to determining the type and content of the surfactants. In this study, the effects of different kinds of surfactants such as CA, SDS, SDBS, SLS and PEI on the electrophoretic deposition behavior of nanoparticles were investigated. The PEI showed superior dispersibility was chose to be the additive. Subsequently, the content of PEI was discussed.

After determining the appropriate additive, the electrophoretic deposition kinetics of Al, CuO and Al/CuO were explored at different electrophoretic times at field strength of 100 V/cm, 150 V/cm, and 200 V/cm. The relationship between current density and deposition time during electrophoresis was recorded.

2.3 Preparation of Al/CuO energetic materials

The Al/CuO energetic materials were prepared by electrophoretic deposition mentioned above. The PEI with a content of 10 wt.% was used as additive. In order to characterize the exothermic performance, the Al/CuO energetic materials with different equivalent ratios were prepared at a field strength of 100 V/cm and a deposition time of 10 min. The equivalent ratios of Al and CuO were 0.75, 1.5, 2.25, 3.0 and 3.75. As equation (1) shows, the equivalent ratio of Al/CuO energetic materials can be calculated by dividing the actual molar ratio of Al to CuO by the theoretical molar ratio of Al to CuO. As shown in equation (2), the theoretical reaction ratio of Al:CuO is 2:3, and the theoretical heat output is 4075 J/g [30].

$$\Phi = \frac{(Al/CuO)_{actual}}{(Al/CuO)_{stoich}} \qquad (1)$$

$$2Al + 3CuO \rightarrow Al_2O_3 + 3Cu \qquad \Delta H = -4075 \ J/g \qquad (2)$$

2.4 Characterization

The composition of the sample was characterized by X-ray diffraction (XRD). The surface elements and chemical states of the Al/CuO energetic composites were analyzed by the X-ray photoelectron spectroscopy (XPS). The morphology of CuO and Al/CuO energetic materials were characterized by scanning electron microscopy (SEM) and energy dispersive spectroscopy (EDS). The heat output of Al/CuO energetic materials were measured by differential scanning calorimeter (DSC). The spectra of Al/CuO energetic materials were characterized by optical fiber spectrometer.

3. RESULTS AND DISCUSSION

3.1 Characterization of CuO microboxes

Figure 1 shows the SEM diagram of the as–prepared CuO microboxes. The CuO is a cubic

microchip with uniform size and a diameter of about 2 μm.
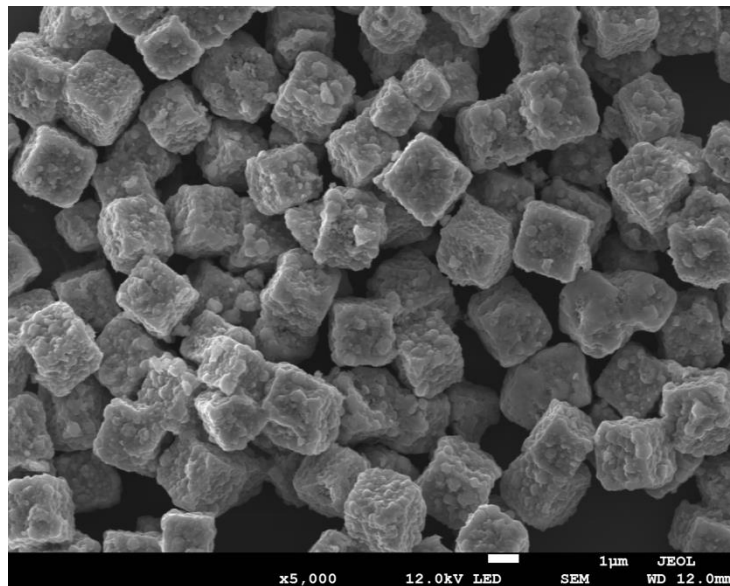

Figure 1. The SEM image of CuO microboxes.

Further, the phase components of the as–prepared CuO microboxes were further analyzed by XRD. Figure 2 is an XRD pattern of as–prepared CuO sample after calcination at 600 °C for 12 h. The diffraction peaks at 32.54°, 35.57°, 38.72°, 48.79°, 53.46°, 58.29°, 61.56°, 66.29° and 68.11° correspond to the standard card of CuO (JCPDS 89–5895). The results showed that the sample calcined at 600 °C for 12 h in an air atmosphere was pure phase CuO.
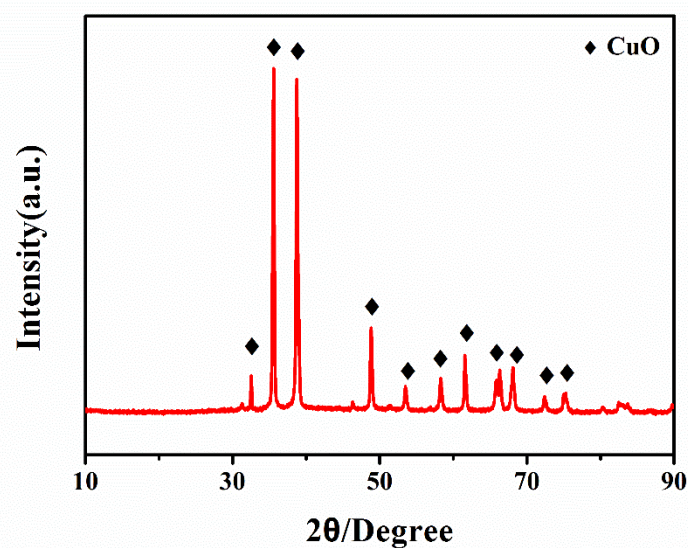

Figure 2. XRD pattern of CuO microboxes.

3.2 Effect of surfactant on the EPD of CuO microboxes

It was found that the as–prepared CuO microboxes could not be deposited on the electrodes by

EPD without additives. Therefore, we further explored the deposition of CuO microboxes under several different additives, including CA, SDS, SDBS, SLS and PEI. The Ti sheets were used as electrodes, and the field strength of EPD was 100 V/cm, and the deposition time was 10 min. The deposition mass of the CuO microboxes were obtained by weighing the Ti electrodes before and after EPD by a precision balance. Table 1 shows the deposition mass of CuO microboxes with different additives. The deposition mass of the corresponding CuO microboxes are the highest after adding PEI. Therefore, PEI was used as additive in the following EPD kinetics study.

Table 1. Deposited mass of CuO microboxes under different surfactants

Surfactant	Surfactant concentration (dwb)	Particle concentration /g·L^{-1}	Deposited mass of CuO/mg·cm^{-2}
Blank	0	1.0	0.00
Citric acid (CA)	10%	1.0	0.00
Sodium dodecyl sulfonate (SDS)	10%	1.0	0.00
Sodium dodecylbenzene sulfonate (SDBS)	10%	1.0	0.17
Sodium lauryl sulfate (SLS)	10%	1.0	1.03
Polyethyleneimine (PEI)	10%	1.0	4.93

We further investigated the effect of PEI content in suspension on the deposition mass of CuO microboxes. In Figure 3, the deposition mass of CuO microboxes increase continuously within the range of PEI content less than 10%. The PEI adsorbed on the surface of CuO microboxes makes it charged positively and improves the stability of CuO microboxes in suspension. The deposition amount of the CuO microboxes did not increase after the PEI content reached 10%, but decreased slightly. Therefore, the CuO microboxes can be dispersed stably in the electrophoretic solution when PEI content is 10%. Thus, PEI with a content of 10% was used in the further study of electrophoresis kinetics of Al/CuO energetic materials.
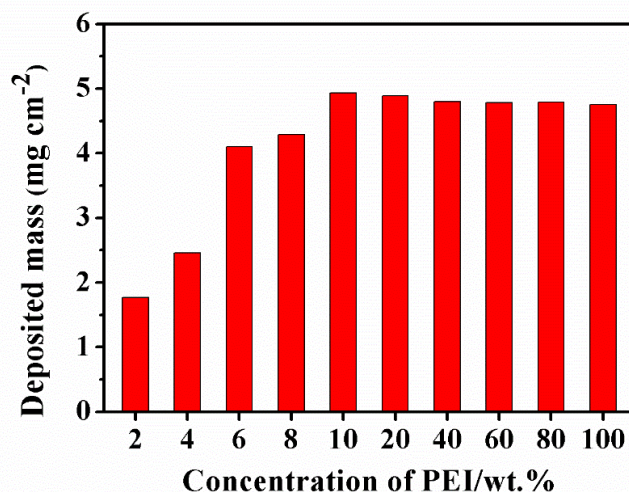

Figure 3. Relationship between CuO deposition mass and PEI content.

3.3 The kinetics of EPD process

The electrophoretic deposition behavior of the CuO microboxes was systematically investigated. The curves of current density with time under three different field strengths of 100 V, 150 V and 200 V were recorded carefully, as shown in Figure 4 (a). The current density decreases with deposition time. As the electrophoresis process progresses, the concentration of CuO particles in the suspension decreases due to deposition and sedimentation. In addition, as the thickness of the deposited film gradually increases, the current density flowing through the electrode decreases. Moreover, the current density is larger at higher field strength, indicating that high field strength enhances the deposition efficiency of the CuO microboxes.

If the EPD process is controlled by diffusion, the current density and the deposition time should obey the Cottrell equation as the equation (3) [31]. The current density and deposition time at different field strength are plotted as the curves shown in Figure 4 (b). Figure 4 (b) shows a good linear relationship between the current density and the reciprocal of the square root of deposition time. The correlation coefficients of the fitting curves are 0.90075, 0.92738 and 0.98634, corresponding to the field strength of 100 V/cm, 150 V/cm and 200 V/cm, respectively. Thus, we can deduce that the EPD process of the CuO microboxes is controlled by diffusion [31-33].

$$i = kc\sqrt{\frac{D_0}{\pi t}} \qquad\qquad (3)$$

Where the i is the current density, k is the constant, c is the initial concentration of the solid particles, D_0 represents the diffusion coefficient and t is the deposition time.
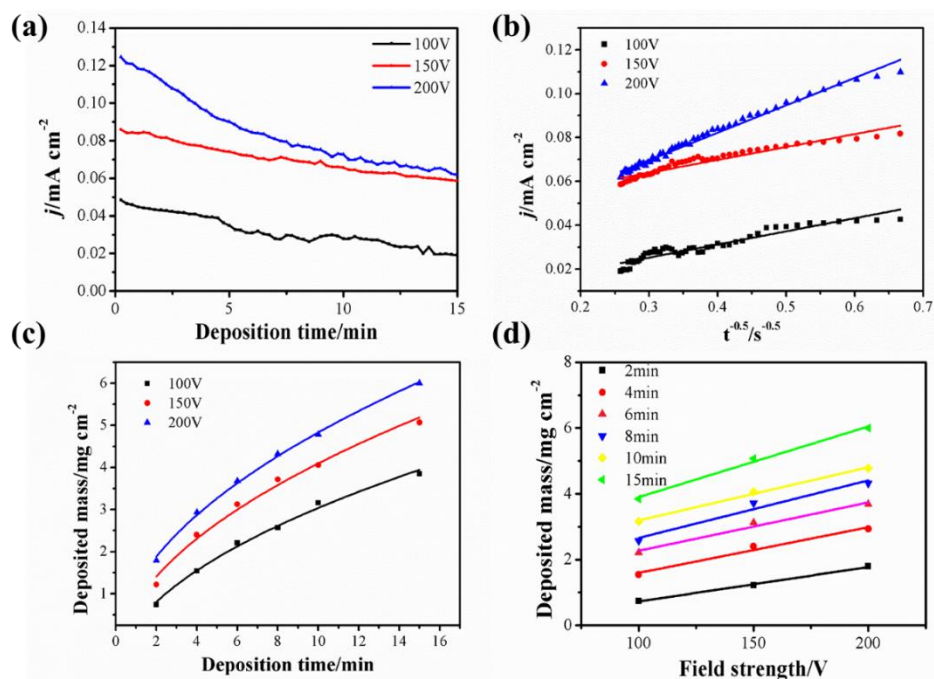

Figure 4. (a) Current density–deposition time curves at three different field strength of 100 V/cm, 150 V/cm, and 200 V/cm, (b) relationship between current density and $t^{-0.5}$ under different field strength in electrophoresis CuO, (c, d) Deposited mass of CuO as a function of deposition time and the field strength.

The deposited mass of CuO microboxes under different EPD conditions were further measured by a precision balance. Figure 4 (c) exhibits the curves of deposited mass and deposition time for three different field strengths of 100 V, 150 V and 200 V. Figure 4 (c) reflects that the deposition mass of CuO microboxes increases with deposition time. The deposition mass and deposition time can be fitted by the following formula (4):

$$Y=a\sqrt{x}+b \qquad (4)$$

Where Y is the deposited mass per unit area, x is the deposition time, a and b are the constant value. The fitting curves shows high R-squared values (Figure 4 (c), $R^2 > 0.98$).

Figure 4 (d) shows the relationship between the deposition amount of CuO microboxes and the field strength at different deposition times. The deposition mass increases linearly with the increase of field strength.
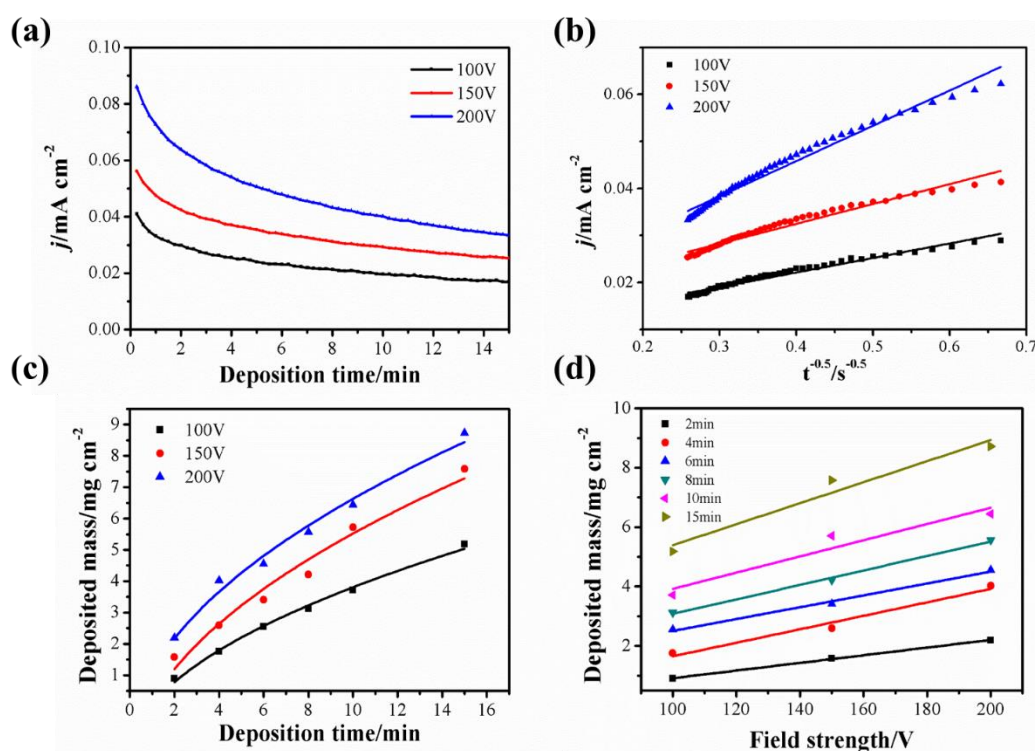

Figure 5. (a) Current density–deposition time curves for three different voltages of 100 V, 150 V, and 200 V, (b) Changes of current density with $t^{-0.5}$ under different voltage in electrophoresis nano-Al, (c, d) Deposited mass of nano-Al as a function of deposition time and the field strength.

The EPD kinetics of the nano-Al particles was also explored for comparison. As is shown in Figure 5 (a) and (b), the current density decreases with the deposition time, suggesting the same regulation with the EPD process of the CuO microboxes. The correlation coefficients between the current density and the reciprocal of the square root of deposition time are 0.97193, 0.96625, and 0.97744, corresponding to the field strength of 100 V/cm, 150 V/cm and 200 V/cm, respectively. Therefore, we can consider that the EPD process of nano-Al particles is also controlled by diffusion [31-33].

The relationship between deposited mass of the nano-Al particles and deposition time under

different voltage is plotted in the Figure 5 (c). The fitting curves are parabolic, and the relativity is preferable with the R^2 values larger than 0.96. Besides, a higher voltage can promote the deposition efficiency. Converting the horizontal axis to field strength, as Figure 5 (d) shows, the deposited mass is in direct proportion to the field strength.

Lastly, the electrophoretic deposition behavior of the Al/CuO energetic materials was investigated. The curves of current density with time under three different field strengths of 100 V, 150 V and 200 V were recorded carefully, as shown in Figure 6 (a). The current density decreases with deposition time. Then, the current density is plotted against the verse of the square root of deposition time, as the Figure 6 (b) shows. According to the equation (3), the correlation coefficients of the fitting curves are 0.86574 (voltage of 100 V), 0.95312 (voltage of 100 V) and 0.96701 (voltage of 100 V), respectively, indicating that the electrophoretic deposition behavior of the Al/CuO energetic materials is mainly controlled by diffusion [31-33].

The deposited mass of Al/CuO energetic materials under different EPD conditions were also measured by a precision balance. Figure 6 (c) exhibits the curves of deposited mass and deposition time under three different field strengths of 100 V, 150 V and 200 V. Figure 6 (c) reflects that the deposition mass of Al/CuO energetic materials increases with deposition time. The deposited mass and deposition time exhibit parabolic–like curve, with R^2 values of the fitting curve larger than 0.96.

Figure 6 (d) shows the relationship between the deposition amount of Al/CuO energetic materials and the field strength at different deposition times. The deposition mass of Al/CuO increases linearly with the increase of field strength.

In this work, experimental results show that the EPD process of CuO microboxes, nano-Al particles and Al/CuO energetic materials is mainly controlled by diffusion. From our previous work [34], the parabolic model of the EPD process has been theoretically deduced. The deposited mass can be regulated by the deposition time and the field strength. Khoo [32] also used the parabolic model to explain that the EPD process of the WO_3 nanorobs was diffusion controlled. In addition to the parabolic model, researchers have built other models like linear model and logarithm model. Guo [35] prepared the tri-dimensional Ni/Al coatings by EPD method. The deposit weight of Al NPs had a good linear relationship with the deposition time. However, this conclusion is only suitable for a short deposition time (within 60 s). Sullivan [33] used EPD to prepare well-mixed energetic composite systems. In the EPD kinetics study, the deposited mass as a function of the deposition time was fitted to a logarithmic curve, while the relationship between the deposited mass and field strength was linear.
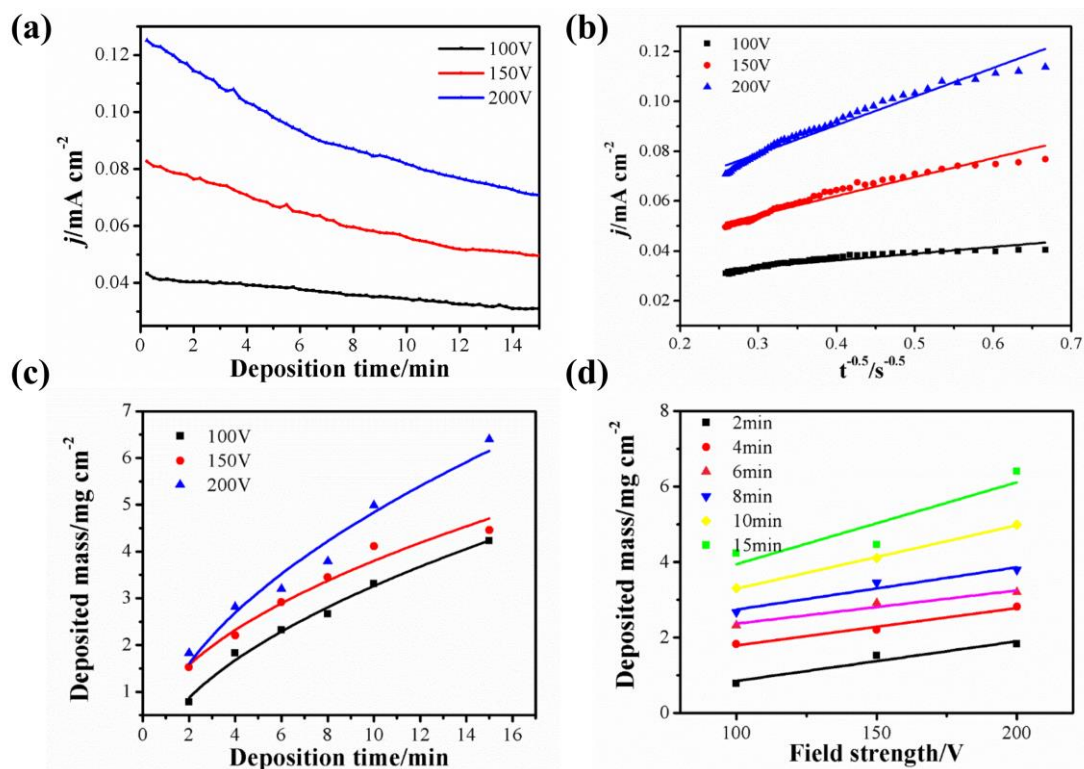
Figure 6. (a) Current density–deposition time curves for three different voltages of 100 V, 150 V, and 200 V, (b) Changes of current density with t$^{-0.5}$ under different voltage in electrophoresis Al/CuO, (c, d) Deposited mass of Al/CuO as a function of deposition time and the field strength.

3.4 Characteristics of Al/CuO energetic materials

The phase composition of Al/CuO energetic materials was analyzed by XRD. Figure 7 is an XRD pattern of Al/CuO energetic materials prepared by EPD. The diffraction peaks in Figure 7 correspond to the Al diffraction peaks (JCPDS No. 89–2769) and the diffraction peaks of CuO (JCPDS No. 45–0973). The absence of Al_2O_3 diffraction peaks and other heterogeneous peaks indicates that both Al and CuO are successfully deposited on the Ti electrode. Besides, the deposited Al and CuO did not react during EPD process.

The surface elements and chemical states of the Al/CuO energetic composites were analyzed by the XPS. Figure 8 shows the survey and high solution scans of XPS spectra. From the Figure 8 (a), the Al/CuO energetic composite contains Al, Cu, O, C and N five elements. The binding energy of 74 eV, 531 eV, 284 eV and 399 eV correlates to the Al 2p, O 1s, C 1s and N 1s respectively. The peak ranging from 979 eV to 933 eV represents the Cu 2p. Figure 8 (b)-(f) shows the high solution spectra of Al 2p, Cu 2p, O 1s, C 1s and N 1s. As observed in Figure 8 (b), the binding energy of Al 2p is 74.1 eV, which may ascribe to the oxidation of Al in the surface. In Figure 8 (b), the peaks at 952.8 eV and 932.7 eV are 2p 1/2 and 2p 3/2 of Cu. Furthermore, the shake-up peaks in 961.9 eV and 932.7 eV indicate the existence of CuO. In Figure 8 (e) and (f), the peaks of C (284.4 eV) and N (399.4 eV) derive from the C-N bond of PEI.
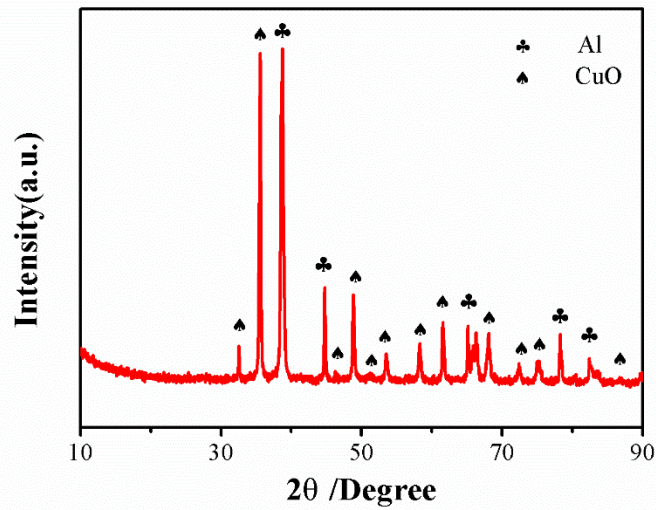
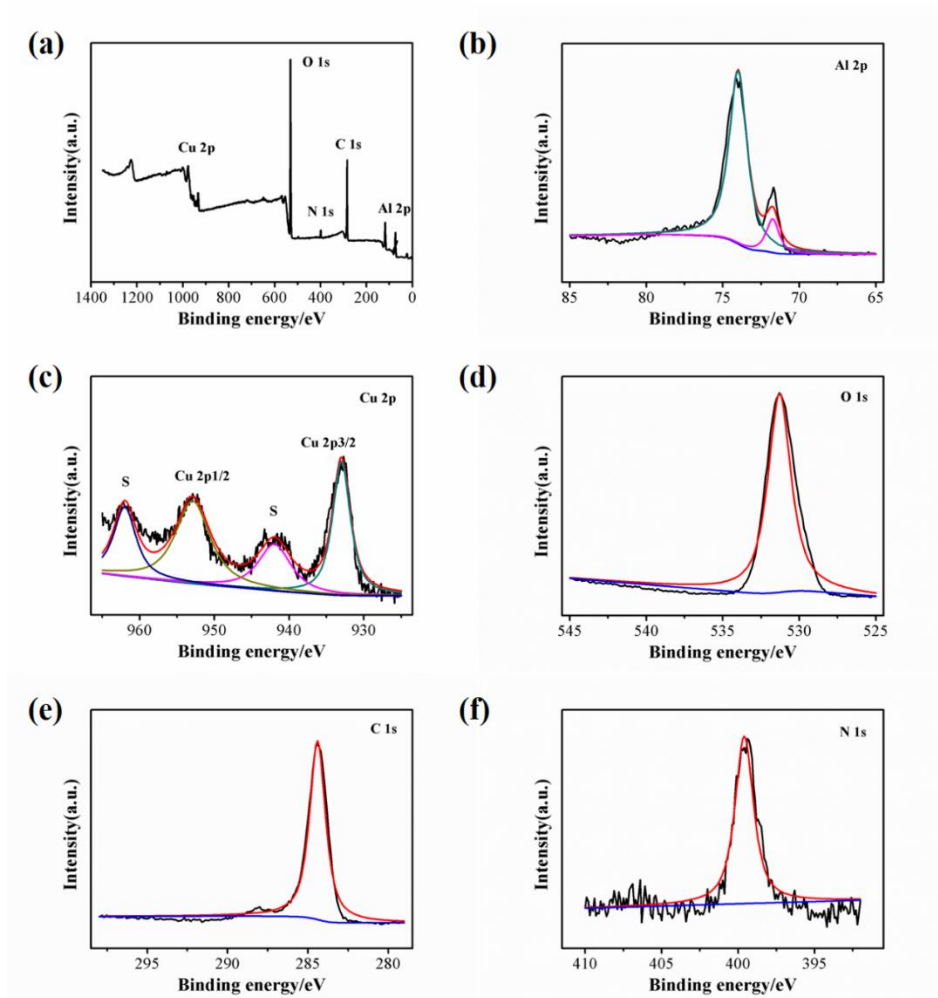**Figure 7.** XRD pattern of Al/CuO energetic materials prepared by EPD.

Figure 8. The survey and high resolution scans of XPS spectra of Al/CuO energetic material: (a) survey spectra, (b) Al 2p spectra, (c) Cu 2p spectra and the S represents shake- up peak, (d) O 1s spectra, (e) C 1s spectra and (f) N 1s spectra.

The micro morphology of nano–Al, CuO microboxes and Al/CuO energetic materials were further analyzed by SEM. Figure 9 (a) shows a SEM image of spherical nano–Al with uniform particle size. In addition, the CuO microboxes prepared in this study also showed uniform size. Figure 9 (c) is a SEM image of Al/CuO prepared by EPD. The nano–Al and CuO microboxes are uniformly distributed together. As shown in Figure 9 (d–f), the corresponding elemental mapping of Al/CuO energetic materials further proves the uniform distribution of Al, Cu and O elements. In particular, this uniformly distributed structure results in uniform mixing of nano–Al and CuO microboxes, enhancing the exothermic properties of Al/CuO energetic materials.
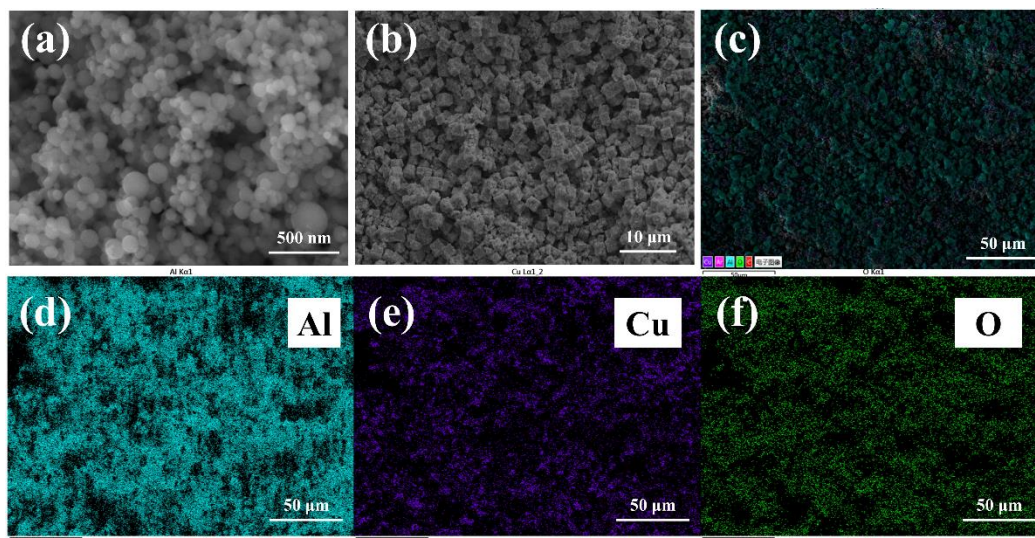

Figure 9. The SEM images of (a) nano–Al, (b) CuO microboxes and (c) deposited Al/CuO energetic materials. (d–f) the corresponding elemental mapping of Al/CuO energetic materials.

3.5 Exothermic behavior of Al/CuO energetic materials

The equivalence ratio plays a crucial role in the heat release of energetic materials. Figure 10 shows the DSC curves of Al/CuO energetic materials with different equivalence ratios prepared by EPD at 150 V field strength for 10 min. It was observed that exothermic peaks appeared about 549 $^{\circ}$C, corresponding to the solid–solid thermite reaction. The endothermic peak at 650 $^{\circ}$C corresponds to the melting of nano–Al. When the temperature continues to rise, the exothermic peak reappears attributing to the solid–liquid reaction between melted Al and solid CuO.

By integrating DSC curves, the heat release can be calculated to be 2099 J/g (Φ_s=0.75), 2163 J/g (Φ_s=1.5), 2576 J/g (Φ_s=2.25), 3049 J/g (Φ_s=3.0) and 1979 J/g (Φ_s=3.75), respectively. It is noteworthy that Al/CuO energetic materials have the largest heat release at 3049 J/g at Φ_s=3.0.
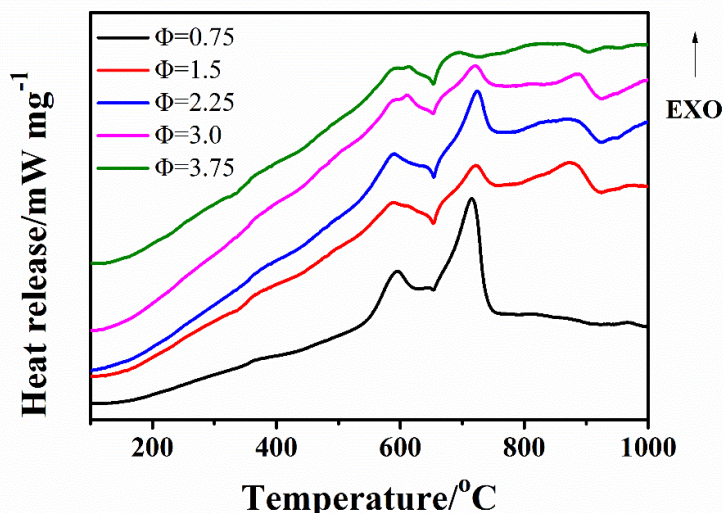
Figure 10. The DSC curve of Al/CuO energetic materials with different equivalence ratios.

Al/CuO energetic materials were ignited by heated resistance wires and their response spectra were recorded by Ocean Optics USB2000. To avoid other light interference, the entire spectroscopy recording experiment was performed in a dark pipeline. The integration time recorded by the optical fiber spectroscopy was 5000 μs, and the distance between the sample and the fiber sensor was 1.2 m. When the suspension equivalent ratio is 2.25 from Figure 11, the Optical fiber spectrum of the Al/CuO energetic material is the strongest. In contrast, Al/CuO energetic material with an equivalent ratio of 3.75 occurs self–propagating melting. Thus, the spectrometer detects the light emitted by the hot resistance wire and the molten thermite.
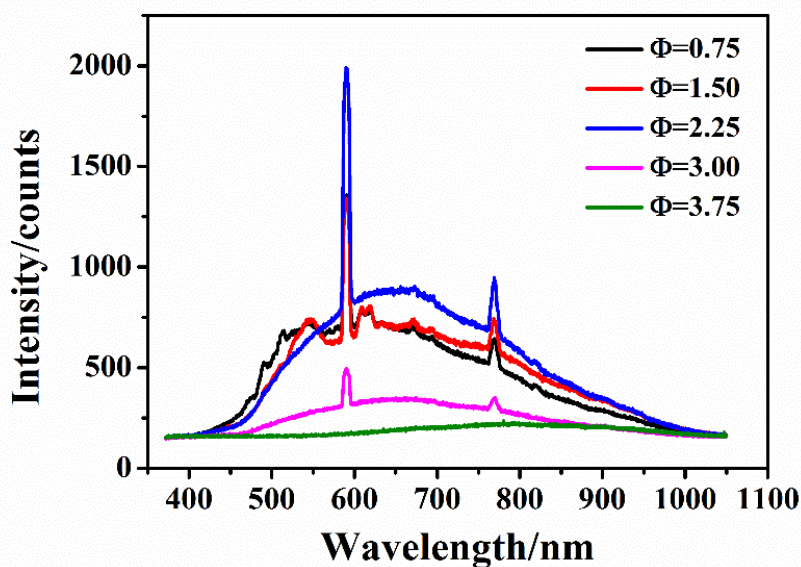

Figure 11. Optical fiber spectrum of Al/CuO energetic materials.

Furthermore, the combustion performance of Al/CuO energetic materials was further evaluated

by the color temperature corresponding to the optical fiber spectrum. The color temperature of the reaction is calculated from the spectrum data and can be used to evaluate the combustion performance of the energetic material.

The horizontal and vertical color coordinates of the spectrum are calculated by introducing the spectral data into the GoCIE software. Then enter the color coordinates into the CIE1931 software to get the position of the color temperature. The color temperature coordinates are substituted into equations (14) and (15) to obtain the color temperature value [36].

$$n=(x–0.3320)/(y–0.1858) \qquad (14)$$
$$T/K= –437n^3+3601n^2–6861n+5514.3 \qquad (15)$$

where T is the color temperature; K and n are the coefficient; x and y are the color coordinate obtained by the GoCIE software.
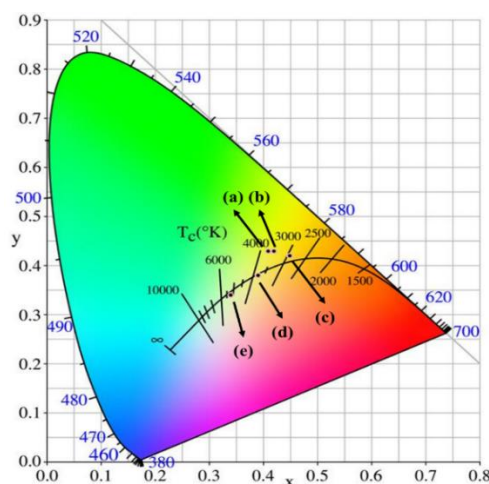

Figure 12. Color temperature map of Al/CuO energetic materials: (a) Φ_s=0.75, (b) Φ_s=1.50, (c) Φ_s=2.25, (d) Φ_s=3.00 and (e) Φ_s=3.75.

Table 2. Color temperature values

Equivalent ratio	x	y	n	T/K
0.75	0.41	0.43	0.32	3676
1.50	0.42	0.43	0.36	3489
2.25	0.45	0.42	0.50	2916
3.00	0.39	0.38	0.35	3775
3.75	0.34	0.34	0.05	5168

Figure 12 shows the location of the color temperature map of the Al/CuO energetic material obtained by the CIE 1931 software. The color temperature values calculated from the data of the optical fiber spectrum are shown in Table 2. When the suspension equivalent ratio is 2.25, the Al/CuO energetic material has the lowest color temperature, and the corresponding film equivalent ratio is 5.94. There is a clear difference between the color temperature and the reaction temperature. It is generally considered

that the color temperature is negatively correlated with the temperature. Therefore, the sample with the strongest reaction has the lowest color temperature of 2916 K.

4. CONCLUSIONS

In summary, a high exothermic Al/CuO energetic material has been successfully prepared in this study. The electrophoretic deposition behavior of Al/CuO energetic materials was studied carefully. It was found that the deposition mass was proportional to the square root of deposition time and the field strength. The electrophoretic deposition process of Al/CuO energetic materials is controlled by diffusion. When the equivalent ratio is 3.0, DSC results exhibit that the maximum heat release of Al/CuO energetic materials is 3049 J/g. The Al/CuO energetic material has the strongest optical fiber spectrum at an equivalent ratio of 2.25, and the color temperature is at a minimum of 2916 K.

References

1. X. Ke, X. Zhou and G. Hao , *Appl. Surf. Sci.*, 407 (2017) 137.
2. J.B. DeLisio, F. Yi, D.A. LaVan and M.R. Zachariah, *J. Phys. Chem. C.*, 121 (2017) 2771.
3. R.T. Mousavian, R.M. Larki and S. Behnamfard, *Mater. Res. Express.*, 6 (2019).
4. L. Qin, N. Yan and J. Li, *RSC Adv.*, 7 (2017) 7188.
5. T.F. Zhang, Z. Wang and G.P. Li, *J. Solid State Chem.*, 230 (2015) 1.
6. J.X. Song, X. Fang and T. Guo, *J. Braz. Chem.* Soc., (2017).
7. Y. Tai, J. Xu and F. Wang, *J. Appl. Phys.*, 123 (2018).
8. D. Stamatis, E.L. Dreizin and K. Higa, *J. Propul. Power*, 27 (2011) 1079.
9. N. Quang, C. Huang and M. Schoenitz, *Powder Technol.*, 327 (2018) 368.
10. F. Saceleanu, M. Idir and N. Chaumeix, *Front. Chem.*, 6 (2018) 10.
11. G. Jian, L. Liu and M.R. Zachariah, *Adv. Funct. Mater.*, 23 (2013) 1341.
12. C. Yu, W. Zhang and R. Shen, *Mater. Design*, 110 (2016) 304.
13. K.S. Martirosyan, *J. Mater. Chem.*, 21 (2011) 9400.
14. W. He, B. Tao and Z. Yang, *Chem. Eng. J.,* 369 (2019) 1093.
15. A. Nicollet, G. Lahiner and A. Belisario, *J. Appl. Phys.*, 121 (2017).
16. W. He, P.J. Liu and G.Q. He, *Adv. Mater.*, 30 (2018).
17. L. Glavier, G. Taton and J.-M. Ducéré, *Combust. Flame*, 162 (2015) 1813.
18. H. Wang, J.B. DeLisio and G. Jian, *Combust. Flame*, 162 (2015) 2823.
19. S.G. Hosseini, A. Sheikhpour and M.H. Keshavarz, *Thermochim. Acta*, 626 (2016).
20. Z. Qiao, J. Shen and J. Wang, *Compos. Sci. Technol.*, 107 (2015) 113.
21. Y. Zhu, X. Li and D. Zhang, *Mater. Design*, 109 (2016) 652.
22. R. Takeuchi, T. Sato and T. Masaki, *J. Photoch. Photobio. A.*, 358 (2018) 395.
23. A.A. Daryakenari, D. Hossein and Y.L. Ho, *ACS Apply. Mater. Inter.*, 8 (2016) 15975.
24. S. ChandraKishore, A. Pandurangan, *Appl. Surf. Sci.,* 258 (2012) 7936.
25. Y. Yin, X. Li and Y. Shu, *Mater. Design*, 117 (2017) 104.
26. D. Zhang, X. Li and B. Qin, *Mater. Lett.*, 120 (2014) 224.
27. K. Ilunga, O. del Fabbro and L. Yapi, *Powder Technol.*, 205 (2011) 97.
28. Q. Wang, Y. Ma and Y. Wang, *Nanotechnology*, 31 (2020).
29. Z. Zhang, H. Che and J. Gao, *Catal. Sci. Technol.*, 2 (2012) 1207.
30. S. Elbasuney, M.G. Zaky and M. Radwan, *Appl. Surf. Sci.*, 419 (2017) 328.
31. N. Koura, T. Tsukamoto, H. Shoji, et al. *Jpn. J. Appl. Phys.*, 34 (1995) 1643.

32. E. Khoo, P.S. Lee and J. Ma, *J. Eur. Ceram. Soc*., 30 (2010) 1139.
33. K.T. Sullivan, M.A. Worsley and J.D. Kuntz, *Combust. Flame*, 159 (2012) 2210.
34. Q. Wang, B. Xing, X. Guo, *Vacuum*, 167 (2019) 244.
35. X. Guo, X. Li, Z. Wei, *Appl. Surf. Sci.*, 387 (2016) 8.
36. C. Manjunath, M.S. Rudresha and B.M. Walsh, *J. Lumin*., 211 (2019) 437.